A study into the effect of different nozzles shapes and fibre-reinforcement in 3D printed mortar

Dr. Pshtiwan Shakor

Abstract

Recently, 3D Printing has become one of the most popular additive manufacturing technologies. This technology has been utilised to prototype trial and produced components for various applications, such as fashion, food, automotive, medical and construction. In recent years, automation also has become increasingly prevalent in the construction field. Extrusion printing is the most successful method to print cementitious materials, but it still faces significant challenges, such as pumpability of materials, buildability, consistency in the materials, flowability and workability. This paper investigates the properties of 3D printed fibre-reinforced cementitious mortar prisms and members in conjunction with automation to achieve the optimum mechanical strength of printed mortar and to obtain suitable flowability and consistent workability for the mixed cementitious mortar during the printing process. This study also considered the necessary trial tests, which are required to check the mechanical properties and behaviour of the proportions of the cementitious mix. Mechanical strength was measured and shown to increase when the samples were printed using fibre-reinforced mortar by means of a caulking gun, compared with the samples that were printed using the same mix delivered by a progressive cavity pump to a 6 degree-of-freedom robot. The flexural strength of the four-printed layer fibre-reinforced mortar was found to be 3.44±0.11MPa and 5.78±0.02MPa for the one-layer. Moreover, the mortar with different types of nozzles by means of caulking is printed and compared. Several experimental tests for the fresh state of the mortar were conducted and are discussed.

Keywords

Extrusion printing, cement mortar, mechanical properties, fibre reinforced printed object.

1 INTRODUCTION

Automation processes have contributed significantly to industrial fabrication and economic aspects of production. The construction industry has limited automation when compared with other industrialized sectors, such as manufacturing. By developing additive manufacturing processes, construction companies could potentially increase revenue and productivity, whilst simultaneously improving safety. There is evidence that automated machinery plays a crucial role in regulating time management and is less costly and more eco-friendly ([1]; [2]; [3]; [4]; [5]; [6]).

It is obvious that Additive Manufacturing (AM) can play a positive role in construction applications. In AM, the two most popular techniques of three-dimensional Printing (3DP) are ink-jet printing (powder-based or binder jet) and extrusion printing/plotting (extrusion-based process). They are the most widespread techniques in construction [7]. These two techniques are shown in Figure (1). Particularly, the AM for 3DP powder-bed process has been divided into three sectors have been recognized [8], i) selective binder (cement) activation, ii) binder jetting and iii) selective paste intrusion.

The extrusion printing technique consists of an extruder which extrudes cementitious slurry through a nozzle attached to a frame to print a layered structure. The first example of this technique in the construction field was Concrete Printing which was proposed by [9], [10] and Contour Crafting established by [11].

The inkjet 3DP technique can be utilised for construction purposes. Christ, et al. [12] incorporated polyacrylonitrile fibre fillers into the printed gypsum element to fabricate a reinforced scaffold.

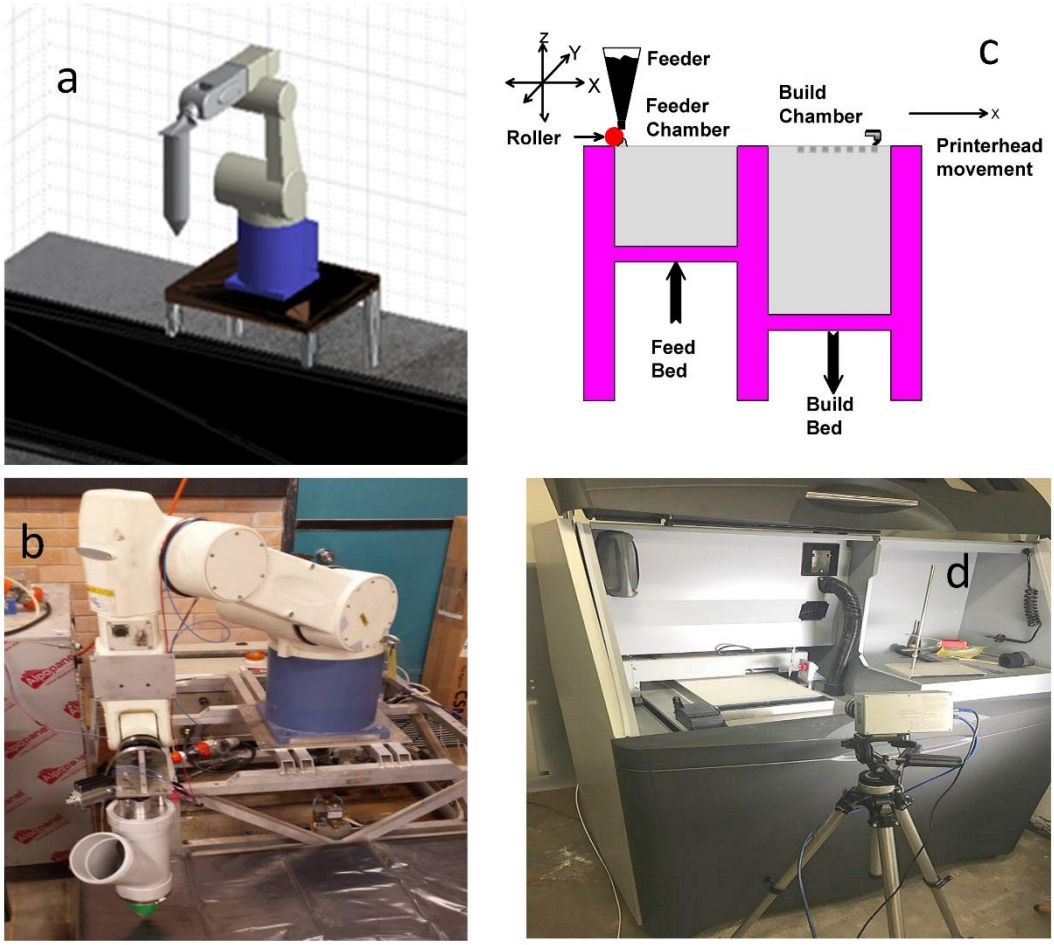

Figure (1) (a) Robot simulation, with the nozzle assembly attached, used to demonstrate the motion plans and check for potential collisions or undesirable paths; (b) Real-world robot with attached auger nozzle assembly; (c) Schematic demonstration of the inkjet 3DP process; (d) Real inkjet 3DP.

Most recent studies on the fibre reinforced printed mortar and concrete, the lightweight cellular composite structures [13], the epoxy-based ink was used to enable the printing of cellular composites with a high-aspect ratio of fibre reinforcement to make a hierarchical structure using balsa wood. There are a few recent studies on fibre-reinforced cementitious materials [14], which investigated mixing Portland cement with short fibres of carbon, glass and basalt (3-6 mm). The mix design consisted of 61.5% weight of Portland cement, 21% of silica fume, 15% of water and 2.5% of the water reducer agent. The retarder (Pantarhol 85, Pferrer) was added (0.3% by weight of a hydration inhibitor) to reduce cement thickening while printing. The results of this study showed that the highest flexural strength was 30 MPa and compressive strength was 80 MPa. Another study that has been worked on the strain-hardening cement-based composites with high-density polyethene microfibers (HDPE) with a length of 6 mm and diameter 0.012 mm [15]. They

found that 1% and 1.5% of HDPE fibre suitable for the printed application with notice of the 1.5% HDPE fibre in the cement-base created higher strain capacity higher and could distribute uniformly. In the study by [7], it has mentioned that the different shape of extrusion nozzles used in earlier works (i.e, circular, ovular or rectangular) but there are not any clear for differences among the nozzles. Another study, discuss to attain the buildable layers and required shape, it required to have an appropriate nozzle [16] [17]. They mentioned that the nozzle orientation of the nozzle and various shape of the nozzle (i.e. circular, ellipse, square and rectangular) has been used and argues that the circular nozzle gives more freedom and easily change the angle of the printed part [16]. The study by Kwon [4] concluded that the square orifice or nozzle has a better surface finish than the ellipse type. Another study by [18] has been used the circular nozzle with various diameters of 4 to 22mm, then the optimum diameter for their study was 9mm.

There are few studies that cover concrete mix design proportions for 3DP in the literature. However, one of the studies that used concrete mix printing through the extrusion methodology is that of [19]. They prepared a cement-based mortar consisting of silica fume, cement, sand, polypropylene fibre and fly ash as the main ingredients. The optimum concrete mix design for the study was shown to be silica fume 83, cement 579, sand 1241, fly ash 165, and water 232 (kg/m^3). Le et al. (2012) scrutinized the mechanical properties of high-performance printed concrete by using a 9 mm diameter nozzle. The resulting compressive strength in different directions was between 75 and 102 MPa for the printed samples. Researchers have also used gypsum [18], where the mix of gypsum and cement are optimised for the 3DP, with experimental tests of compressive strength of 100-110 MPa being achieved. Lim, Buswell, Le, Wackrow, Austin, Gibb and Thorpe [18] used the short delivery method by placing the hopper on the top of the extruder. They also used the small batches of materials to control the hardening of the mix. There is a study on the 3DP earth-based materials using alginate as a fast setting binder by mean of 6 DOF robot to print circular shape and rectangular shape earth-based samples [20]. They observed voids in circular cross-section; contrarily, the rectangular cross-section absence of cavity and voids. It also noticed that the compressive strength in rectangular cross-section higher than the circular cross-section.

The earlier study by Gosselin, et al. [21] used two peristaltic pumps, one for the premixed slurry and the other for the accelerator agent. Earlier studies have used different delivery methods and different mixing processes which have a significant effect on the printed product in terms of workability, shapability and mechanical strength. Le, Austin, Lim, Buswell, Gibb and Thorpe [9] have used a hopper conveyed by a pipe to the CNC machine to print the slurry of the concrete. They faced issues regarding the cohesiveness of the mixing, such as high sand content.

In the present paper also discussed an investigation of the delivery system to print the objects. As a

result, the current study investigated the use of different delivery conveyors and their effect on the final result of the fabricated concrete.

The present paper focuses on validating the optimum mix proportion, which can be delivered using different delivery sources to print the cementitious slurry. The most suitable type of fibre, which flows easily with slurry, was selected. The study compared mechanical behaviours of the printed mortar with and without fibre-reinforcement. This study also discusses the benefit of fibre reinforcement into the mix design of the cementitious material. Fibre-reinforcement has been used in previous studies for different types of construction applications[22] [15] . In this study, fibre filaments has been used to reinforce the cementitious mortar and improve the mechanical performance of the materials.In addition, different types of nozzles have been used and compared.

2 EXPERIMENTAL PROGRAM

2.1 MATERIALS

Materials play a crucial role in 3DP of objects for construction applications. When the properties of the materials are optimised, the printing process will have a better result. In the present work, the materials consisted of fine sand (Sydney Sand) by Australian Native Landscapes, ordinary Portland cement (General Purpose cement) by Eureka and chemical admixtures such as superplasticizer (SikaPlast®3 in 1), accelerator (Sigunit L80AF), and retarder (Retarder N). The accelerator was used to accelerate the setting time of the mortar during printing while retarder agent was used to open time and reduce the thickening of the cement in the delivery system and control rheology of the mortar [23]. Particle size distribution was conducted for the fine sand with a maximum particle size of 300µm. The particle size analysis distribution was prepared using a sieve mesh and particle size analyser. The fibre used was polypropylene (PP) (6mm) (Elasto Plastic Concrete), Table (1).

Table (1) Mechanical properties of the PP fibre that has been used in the mortar mix.

Fibre type	Length /Diameter	Thickness	Specific gravity (g/cm3)	Tensile strength (MPa)	Tensile modulus (GPa)
Polypropylene	6mm	100 µm	0.91	1300	7.2

Figure (2) shows particle size distribution versus the percentage of passing particles of ordinary Portland cement and fine sand which were used in the mortar mix.

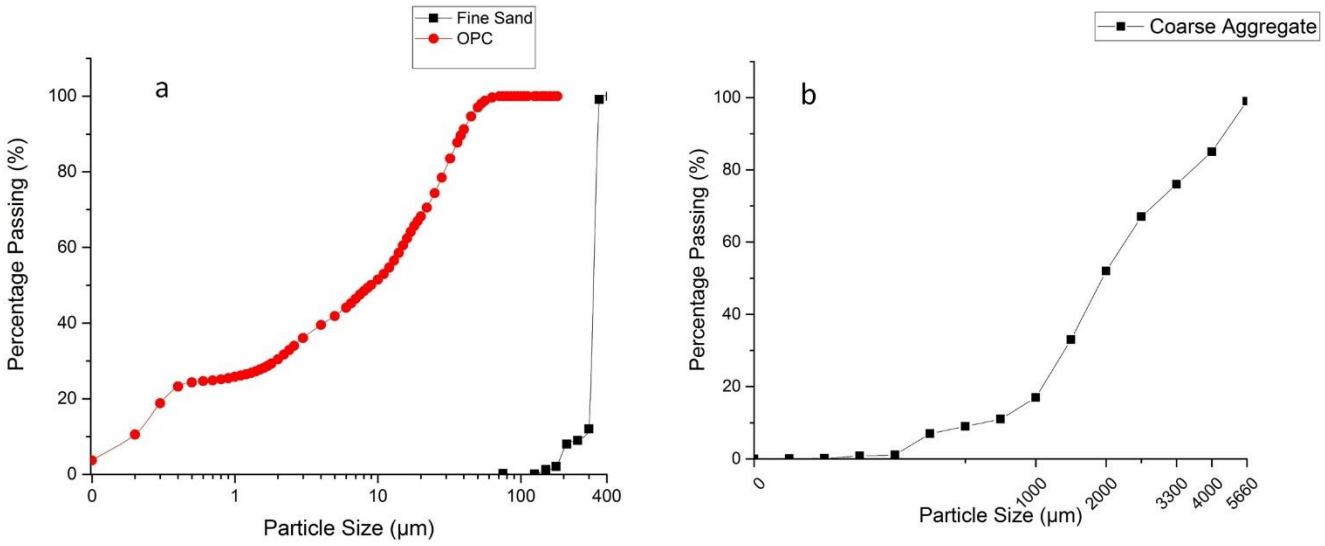

Figure (2) (a) Fine sand and Ordinary Portland Cement particle size distribution, (b) Coarse aggregate particle size distribution .

2.2 DESIGN AND FABRICATION

2.2.1 Extruder adaptation and delivery system

The extruder for the printed mortar shown in Figure (3) was designed so that it could be mounted to the end-effector of an industrial robot. The design, inspired by Anell [24], incorporates improvements to increase the efficiency of printing cementitious materials.

The pump was adopted to appropriately deliver material to the extruder. The extruder consists of the components shown in Figure (3).

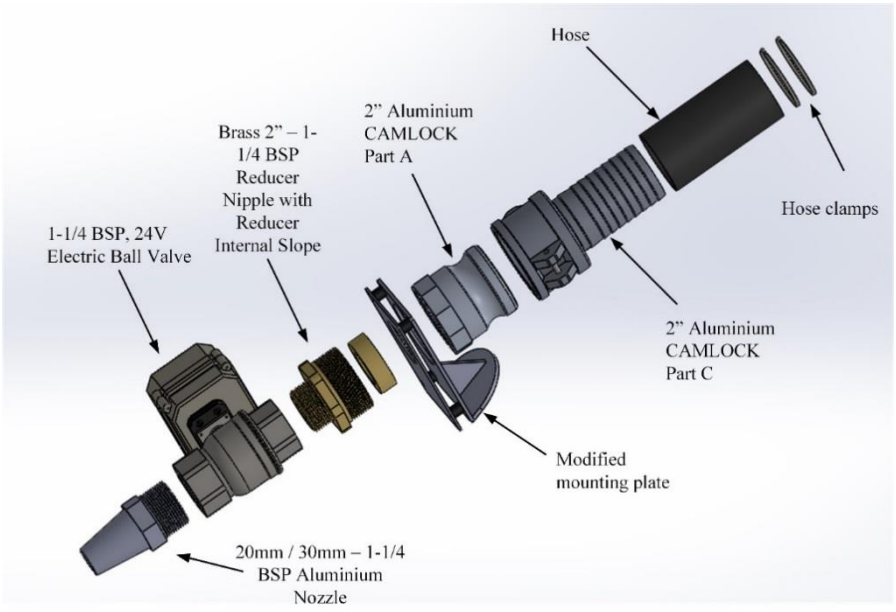

Figure (3) Exploded view of the extruder assembly that is connected to the progressive cavity

pump and is attached to the end of the robot.

A caulking gun was used with different sized nozzles (14mm, 20mm, 35×10mm). The caulking gun has been used in previous work by [25] [26]. The caulking used a mechanically actuated gun to print the cementitious mortar. The progressive cavity pump used a tube with an inner hose with diameters of 20mm and 30mm, see Figure (4).

Figure (4) The final system with the progress cavity pump connected to the robot.

2.2.2 Mix designs for cementitious materials

Several trials for the cement mortar were prepared to check the optimum printable cementitious mortar. Fabrication and mix designs were examined based on previous investigations [27] and further mixed trials were implemented to improve smooth pumpbaility through the pump and delivery systems. Several studies were also prepared for concrete fabrication and printing members. Until now, 3DP concrete and mortar in the construction industry have not been technologically advanced enough and have not been investigated intensively on a large-scale.

The present study fills a gap in the literature by using different mixes until an optimum mix was obtained which could be more compatible with the different delivery system. This study also investigated a suitable delivery method for the printed mortar, while using different mortar mixes to obtain the optimum mix design. Two techniques were adopted to deliver the mortar, namely,

using a caulking gun and a cavity pump.

The mix of mortar with various agents and chemical admixture has vital effects on the air entertainment in the mix, leading to a lot of residual air in the mix. Agents such as superplasticizer, accelerator, retarder and water reducer, affect the percentage rate according to the type of medium and the delivery system. However, for these mixes, the setting time and shapability of the mortar have been considered.

For the caulking gun (internal diameter of nozzle circular 14mm, 20mm, rectangular 35×10mm), several trials are presented in Table (2). Mixing times of 5 to 6 minutes were found to be the most suitable. Due to the inconsistencies of extrusion, printing heights are taken as an average measurement for caulking gun printing. However, the printing height for mortar printing via a robotic arm has been fixed according to the diameter of the nozzle, where the diameter of the nozzle is equal to the height of the end-effector from the printed platform.

Table (2) Mortar mix design with 1 to 1 ratio (cement to sand) with/without fibre.

Trial No.	**Fine Sand (g)**	**Cement (g)**	**Coarse Aggregate (g)**	**Retarder (ml)**	**Accelerator (ml)**	**Water (ml)**	**Superplasticizer (ml)**	**PP Fibre**
T5	375	375	-	2	2.5	125	2.5	0%
T5*	375	375	-	2	2.5	125	2.5	1%
T8	500	500	-	2.66	3.3	171.5	3.33	0%
T12	375	375	125	2	2.5	125	2.5	0%
*selected mix using polypropylene fibre.								

3 FRESH AND HARDENED PROPERTIES TESTS

3.1 FRESH PROPERTIES TESTS

3.1.1 Slump test

The slump tests (spread-flow test) were prepared according to [28] to determine the flowability of the mortar mixes. Essentially, this test was conducted using a mini cone (100×70×50) mm. The first step of the slump procedure is pouring fresh mortar into the mini cone mould and then tamping it slightly, for settling down and levelling purposes, with a manual tamper for approximately 20 tamps.

The conical mould was then filled with the second layer and the third layer using fresh mortar. The

second and third layers were poured and tamped afterwards using the same specified procedure as the first layer. Lastly, the additional paste on the top surface of the conical mould was scraped and flattened. After pouring three layers, the conical mould was lifted and then the height of the specimen was measured. Next, it was subjected to 25 tamps. The diameter of the spreading mortar was then measured in two perpendicular directions. Next, the value of relative slumps was determined using the following equation:

$$rp = (d/d_o)^2 - 1 \quad (1)$$

Where the *rp* is a relative slump, *d* is the average value of two measured perpendicular diameters of the spreading mortar, and d_o equal 100 mm (which is the bottom diameter of the mini-cone).

3.1.2 Squeeze flow test

The squeeze flow test was prepared according to the Brazilian test [29]. For this test, the uniaxial testing machine, Shimadzu (AGS-X 50kN, Japan), was used to check the resistance of three main mixes (see Table (2)) while in a fresh state. The displacement speed was 0.1 mm/second (see Figure (5)). The surface roughness for this test was conducted using a portable profilometer (Taylor Hobson Surtronic 3^+). This test was conducted for the single layers, double layers and triple layers.

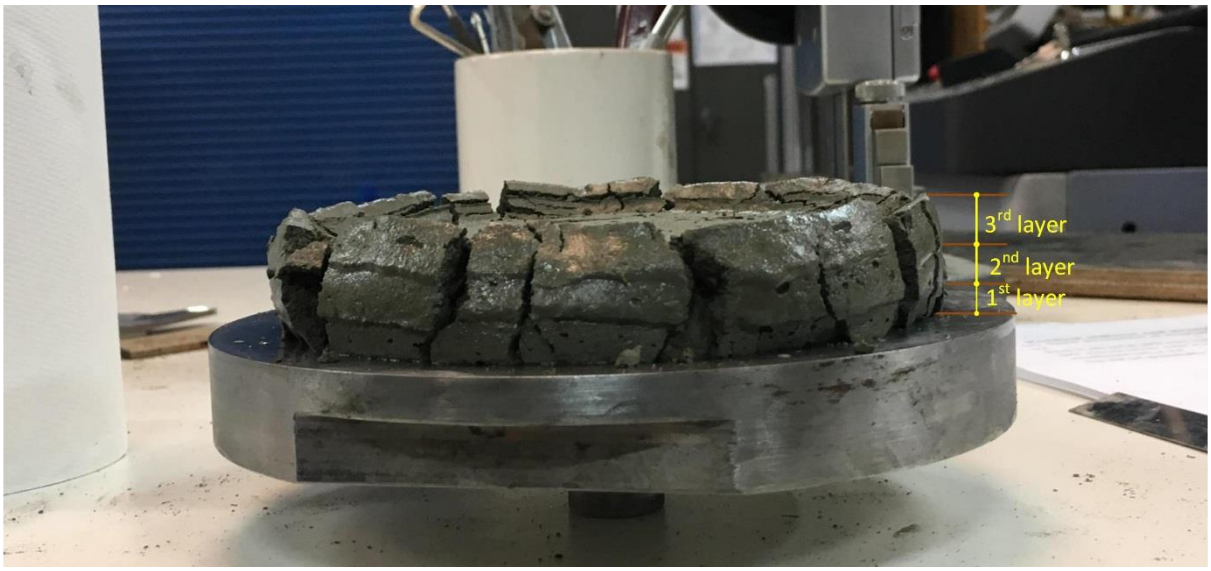

Figure (5) Triple layers of the mortar after squeezing under a uniaxial compression load.

3.1.3 Setting time

The Vicat test was used to validate the layer setting-time of the cementitious materials. In this study, few trials of mortar mix (T5, T8, T12) was selected for a few of these trials and the outcomes are presented in the results section.

The measurement for the Vicat test was implemented according to [30] [31]. The diameter of the needle was 1mm and has a fixed weight of about 300g on a movable rod. A sample of normal uniformity fresh mortar was prepared and placed in a container 40 mm tall. The test consisted of

the measurement of the needle penetration to a required depth which falls due to gravity. The initial setting time was measured every 15 minutes. The first 15 minutes recording of the needle penetration was 39 mm±0.5 mm. The final time recorded less than 0.5 mm of penetration. The setting time test for each printing trial using the caulking gun and the real height and width of the printed layer are listed in the results section. The outcomes and further interpretations are also presented in the results section.

3.2 Hardened Properties Test

Several experiments were conducted to assess the mechanical and hardened properties of materials before printing and during the printing of the components. It is essential to print the small structural members before printing at a larger scale. These tests were prepared based on the mortar materials' behaviours. The mechanical properties of the printed objects are derived by the measurement of the materials' behaviours, which can be used to indicate the yield strength, deformation of the materials and resistance of the materials. Three samples were used for each of the trial and mix designs. Table (3) presents the number of samples and batches.

Table (3) Details of the prepared samples.

Sample description	**Number of the samples**	**Size of samples (mm)**	**Delivery method**
Hollow column	6	(300×300)	Cavity pump
Printed with/without Fibre Reinforced mortar	3	(160×20×12)	Caulking gun (14mm)
	3	(160×20×24)	
	3	(160×20×36)	
	3	(160×20×48)	
Printed with/without Fibre Reinforced mortar	3	(160×20×18)	Caulking gun (20m)
	3	(160×20×36)	
	3	(160×20×54)	
	3	(160×20×72)	
Casted prisms	18	(160×40×40)	Conventional method
Casted cubes	18	(50×50×50)	Conventional method

3.2.1 Compressive strength test

To evaluate the mechanical properties of various mortar mixes, a uniaxial compressive strength test was conducted to check the suitability of the sample under compression before printing the complete components. The cubic specimen dimensions (50×50×50) mm were prepared according to the Australian standard [32]. The loading rate was 0.833 kN/s. The testing machine used was from

Shimadzu (UH-500kN XR 500kN, Japan).

3.2.2 Flexural strength test

To assess the flexural strength of the specimens, a three-point bending test was applied to all the main mortar mixes [33]. The prisms, with dimensions of (160×40×40) mm, were cast for that purpose. The various layers were printed using a caulking gun for the three-point bending test. The gun had the same dimensions as the prism: (160×20×18) mm for one layer; (160×20×36) mm for two layers; (160×20×54) mm for three layers; and (160×20×72) mm for four layers. All used a 20mm circular nozzle. Thus, only the thickness of the sample changed. A similar prism was cast for one, two, three and four layers for a circular nozzle of 14mm. Three samples for each printed layer were prepared. These batches were prepared with fibres and without fibres, see Table (3). The uniaxial testing machine from Shimadzu (AGS-X 50kN, Japan) was used for this test.

4 RESULTS AND DISCUSSION

4.1 MECHANICAL TESTS

Mechanics of materials is dealing with the behave of materials which subject to stresses, this study it can be in the fresh state or hardened state of materials. The mechanical strength test in the presented paper was conducted to measure the fresh slurry o mortar and hardened state of the mortar. Two factors that have a significant effect on the final shape result of the product are (a) the number of printed layers, and (b) the discharging of mortar slurry through different nozzle shapes and sizes.

Figure (7) explains the change in width, which is specified as ($W+\Delta W$), while the thickness is expressed as ($T-\Delta T$). Figure (8) shows that the extruded layers have changed into their original shapes. The first printed layer would also change in width and thickness after loading the next layers. Once again, the first layer will face a change in its shape after the printing of the third layer. This change is possibly continuous until the shape has reached stability in its form and has set enough. The last layer of the component did not encounter any modifications and changes due to no further layers being added, so it retained its own shape, Figure (8).

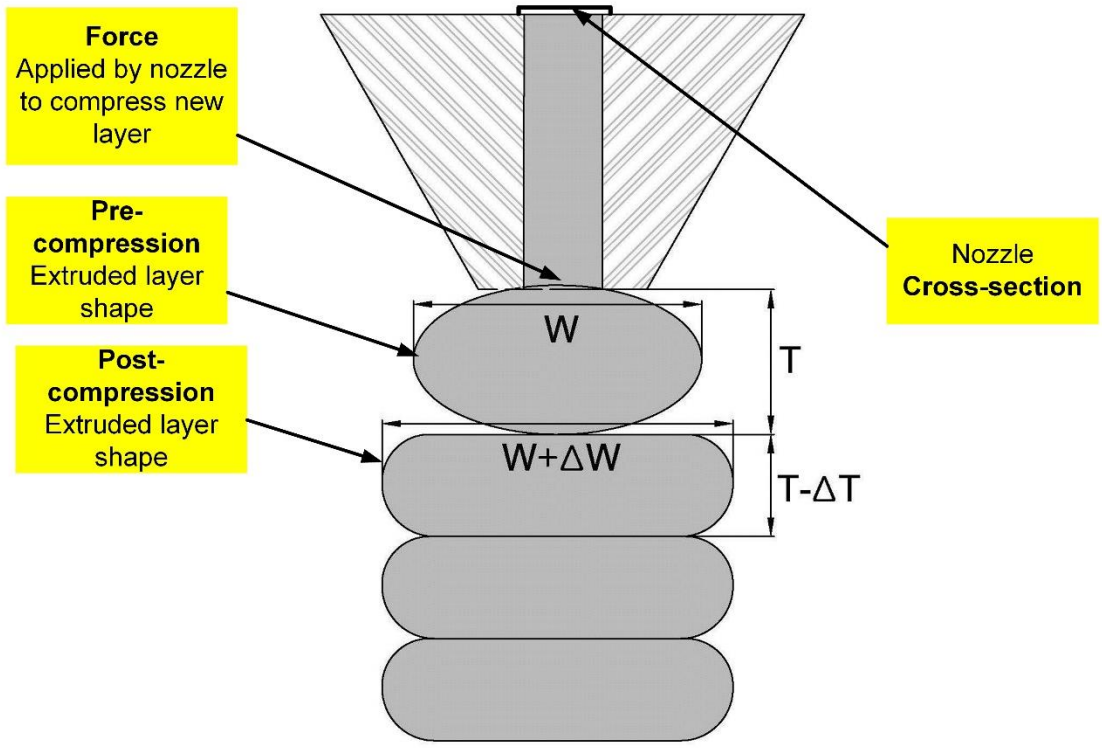

Figure (7) Schematic illustration of the prediction of the printed mortar passed through the circular nozzle.

Where W is the true width and ΔW is the trace width error. T is the true thickness and ΔT is the trace thickness error. Therefore, the area of the object will change at the pre-compression and post-compression stages according to the rheology of the mix proportions and the forced impact by the next layers which are printed. Figure (7) shows that the area of the layers will vary according to the printing height, nozzle types, the mixing time and the setting time of the materials. Therefore, the true area of each cross-section printed layer is equal to $(W+\Delta W)*(T-\Delta T)$.

However, there could be a different result when the time intervals between layers changes. When a slight decrease in the time intervals happens between layers the rate of penetration between layers increases due to the viscosity and shear thickening properties in the concrete. This is consistent with research by Cyr, et al. [35], which found that the shear thinning of the concrete could be changed to shear thickening by adding superplasticizer to the paste of the cementitious materials. Shear thickening is defined as the proportion of the shear stresses to the viscosity of materials which can be increased gradually. This phenomenon emerged during the pumping process of the mortar. The mortar had resisted downward pressure and the viscosity also greatly increased. For this to occur, a mixer in the hopper needs to make a consistent movement in the container. In this study, a different

ratio of superplasticizer was used. This had a significant influence on the setting time of the mortar and the viscosity of the mortar. The ratio of superplasticizer to cement materials was (0.67% to 1%).

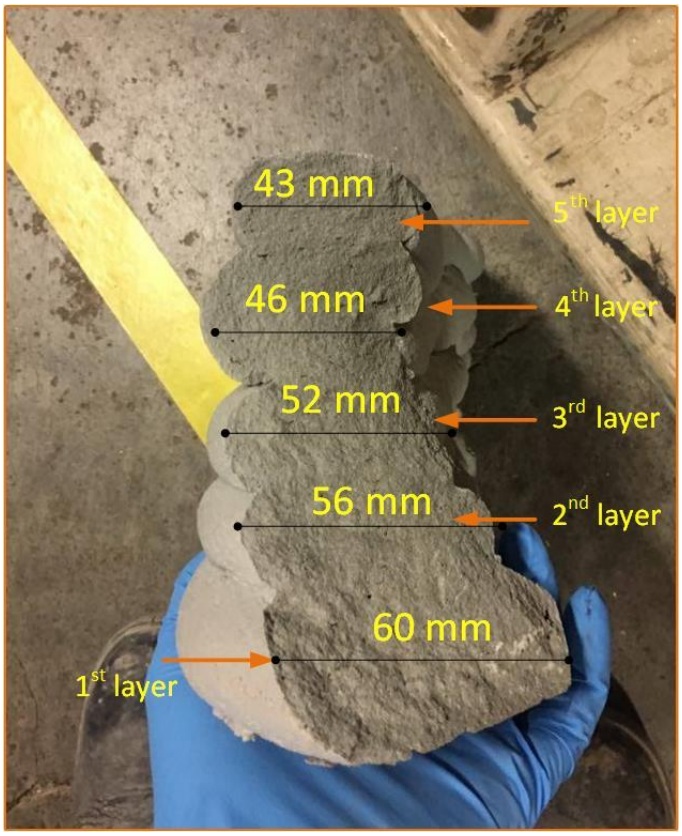

Figure (8) Cross-section of the printed layers details after crushing under a uniaxial compression load.

The shape of the nozzles has an effect on the printability, shape and flowability of the slurry. The study, Li, et al. [36] asserted that intercepting shocks are significantly changed according to the shape of the nozzles. The study found that square shaped orifices are faced with a higher interception than the other jets due to the four corners exiting at the nozzle. In addition, the penetration between two layers increases while the *w/c* and the number of layers increment proportionally. Moreover, the shape of the nozzles also affects the percentage of penetration between the two layers. If the nozzle shape is circular, the penetration rate increased slightly. This is due to less flatness of the previous layer which is laid down as a concave shape. The application of the spherical particles and square particles theory could be applied to the circle and square nozzles in terms of the shape and load applications. Figure (9) shows that the load in the square nozzles is distributed equally due to the radius of distribution in the square shapes. This distribution area is smaller in circular nozzles [37]. Böhmer, et al. [38] found that in the inkjet printing technique the diameter of the droplet, which contains 0.3% polyvinyl alcohol solutions, would be larger than the diameter of the nozzle. They used a different concentration of polymer solution with the three different nozzle diameters.

As a result, at a constant polymer concentration, smaller initial droplets were produced by the smallest nozzle diameter that, in turn, leads to smaller particles as well. Consequently, this could be similar to concrete slurry where a higher flow of slurry is produced with increasing nozzle sizes.
Cwalina, Harrison and Wagner [37] stated that the particles with spherical and cubic shapes produce different results. The squeeze flow and load distribution between two cubic particles and two spherical particles with equivalent radii-lengths are illustrated in Figure (9).
For particles with an identical characteristic half-width, *R*, moving along their lines of centre at a relative velocity, *V*, in a Newtonian fluid of viscosity, *ηf*, the lubrication force between the spherical and cubic particles is given, respectively, as:

$$F_{spheres} = \frac{6\pi V \eta f R2}{h} \quad (4)$$

$$F_{cubes} = \frac{3\pi V \eta f R4}{h3} \quad (5)$$

In the two equations, (4) and (5), it is obvious that the reaction force between two particles increases when the shapes change from cubes to spheres. Therefore, this result will be similar for printing when square or circular nozzles are used. The printed shape will replicate the shape of the nozzles. The particles used in this experimental test were mostly spherical with some of the irregular shapes. As a result, the printed slurry will be a similar shape as it passes through the nozzle. The different shapes and sizes of the nozzles were also investigated in this study. The shapes used were circular and rectangular, with sizes of (20) mm in diameter and (35×10) mm. The forces were distributed evenly over the greater surface area in the square and rectangular shapes than in circular shapes. Consequently, the printed layers of the square or rectangular nozzle shapes withstand more layers than the circular nozzle shapes. It should be noted that the same mix ratio was used for the printed object utilizing different nozzle types. It was found that the nominal width in a rectangular shape was larger by 2±0.85mm than its reduced width (layer surface contact). Conversely, the nominal width of a circular shape was larger by 3.1±0.75mm than its reduced width.
Considering the forces applying to differently shaped particles, the higher forces emerged between flat cubic particle surfaces compared with the curved surfaces characteristic of spherical particles.

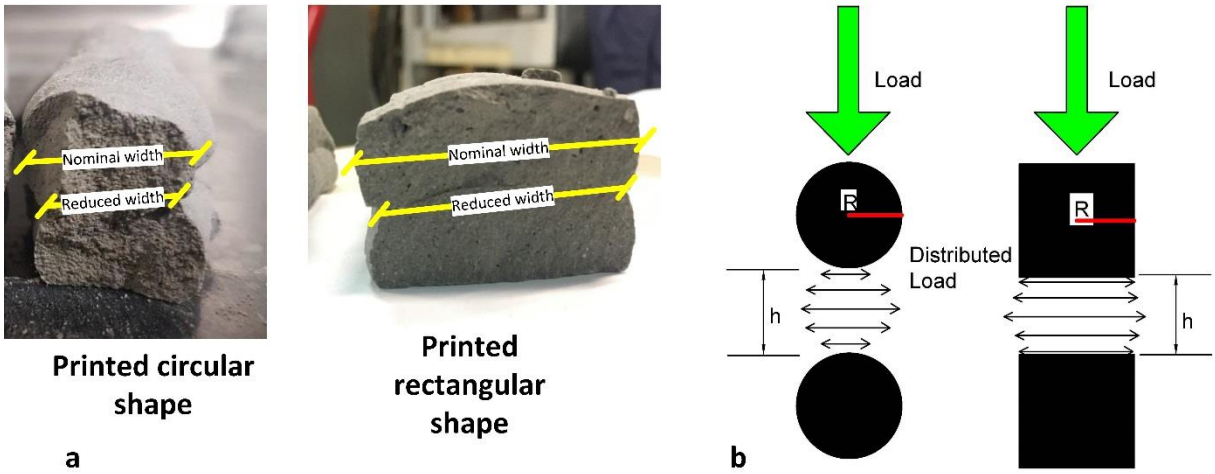

Figure (9) (a) Real printed circular and rectangular shape; (b) Lubrication squeeze flow between two spherical particles (left) and two cubic particles (right) with an identical characteristic half-width, R (reproduced by [37]).

Figure (10), shows an object where one layer has three layers printed onto it. It has been printed to measure its dimensional geometry and test its mechanical behaviour.

Figure (10) (a) Three layers of the printed object; (b) One layer of the printed object.

For a printed object of over 120 mm (more than 7 layers), the oscillation at the arm of the robot increased in the end-tip of the arm which is most related to joint 4 and joint 6 in the robot [27]. Figure (11) shows how the printed layers collapsed after 10 layers of printing.

Figure (11) The movement of the robot arm has a major effect on the printing process, particularly when the height of the object increased to more than 7 layers.

Another challenge that it faced during the printing process was the use of a flat-based hopper, as shown in Figure (12), where core-flow (rat-holing) occurred during the printing of the specimens. It is observed that some of the slurry close to the wall of the bucket is in a static state, while other parts of the slurry are in a mobile state.

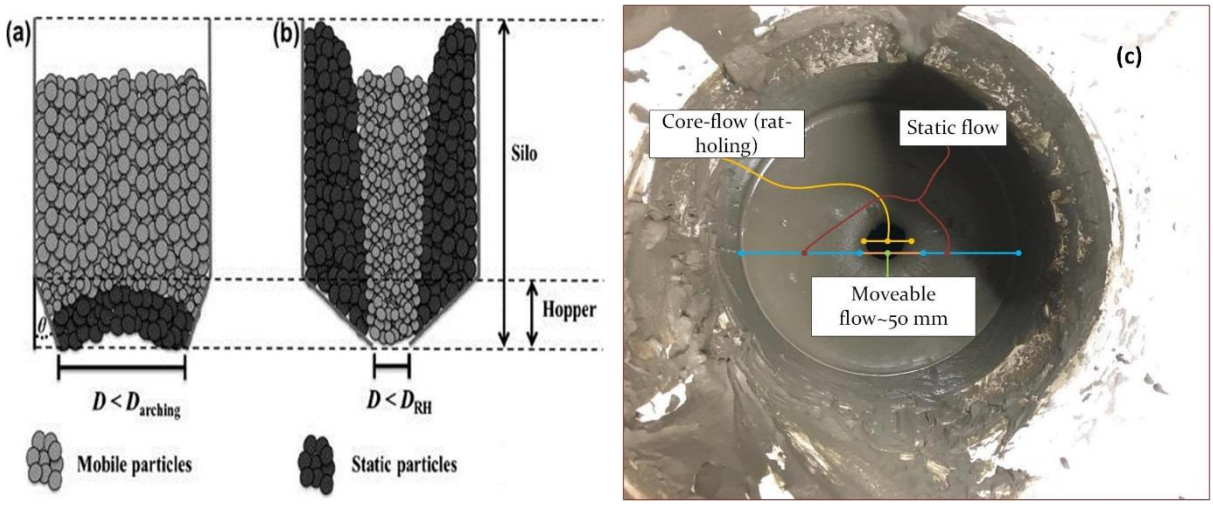

Figure (12) Schematic illustration of flow problems encountered in hoppers, namely, arching and rat-holing, during (a) mass-flow and (b) core-flow, respectively, where D = outlet diameter, $D_{arching}$= minimum arching diameter, DRH = minimum rat-hole diameter and ø = hopper half angle [39], (c) pictorial illustration showed the rat-holing flow in the bucket above the pump during pumping.

Figure (13) shows a modified hopper angle of Ø 45° to improve the flowability in the hopper. Generally, fresh concrete during poured in place behaves as a liquid slurry (a viscoplastic fluid with high yield stress). However, the internal structure of slow casting concrete or when in a rest state leads it to flocculate. It also has the ability to resist the load from concrete cast over it without increasing lateral stress, despite the nature of the mould. Feys, et al. [40] explained that the (hydro-) clusters are assembled together and become moulded from certain shear stress on the critical shear stress. By increasing the shear rate, the viscosity of concrete increases proportionally. This state of fresh concrete is called shear thickening. For the concrete properties, it is noticeable that when the temperature rises, the workability and slump of the concrete decreases. This is another reason that the mortar could not pass through the hopper effortlessly. Apparently, the longer concrete or mortar remains in the hopper, the more advanced the reaction and the higher the increase in temperature, which subsequently leads to an increase in the viscosity of the mortar. A temperature rises from 21°C to 35°C was measured after 30 minutes of the mixing process occurring.

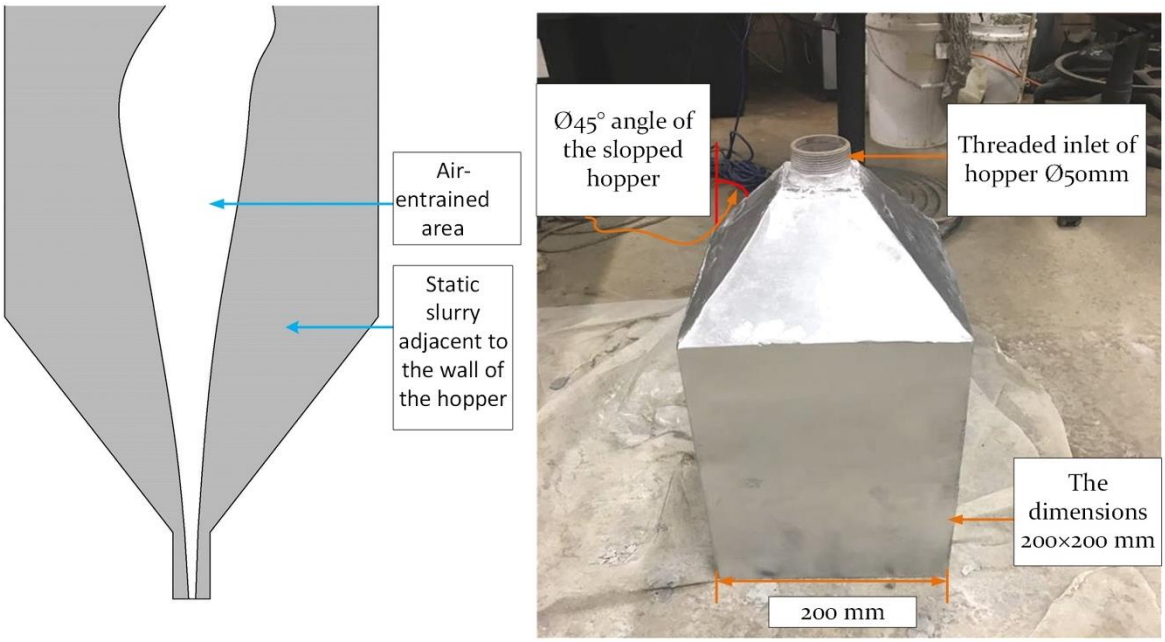

Figure (13) The hopper with an angle of Ø45˚ and the core-flow concept.

Earlier studies explained the two types of powder flow pattern in the hopper: mass-flow and core-flow [39]. The most noteworthy is the core-flow that emerges while feeding the concrete through the pump (deliver) to the robot. According to Fitzpatrick, et al. [41], the moisture content has a high impact on powder particles in terms of flowability. Consequently, the surface forces between the powder particles or slurry and the wall surface play a major role in shaping the nature of the powder flow, see Figure (12).

Figure (13) shows a hopper with an angle of Ø 45°, which reduced rat-holing but did not eliminate it completely. This rat-holing phenomenon happens due to the flocculates of the particles and maintains particles in the static state. Improving this situation requires consistent mixing in the hopper.

For most of the trials that were prepared in the experimental program, a set of prisms and cubes were prepared to validate the mechanical behaviour of the mixing property. The printed prisms have been created by selected trial 5 cementitious mortar as a mix proportions. So, the printed mortar has been tested for each of the layers from (1 to 4) by caulking gun.

The outcomes suggest that a waiting time between layers of 10 minutes is necessary and the ratios of water to admixture need further investigation.

The printed part is shown in Figure (14). Shrinkage cracks appeared on the printed part after one day of curing in the laboratory temperature environment. To reduce the cracks so the printed materials are stronger and exhibit fewer shrinkage cracks, chopped strand fibre was introduced.

Figure (14) (a) The printed part immediately after printing; (b) The printed part after one-day drying.

4.1.1 Slump test

This test showed the different results of the three different trial mixes which have three various slump results. This difference in results was based on their *w/c* mix ratio and the cohesiveness of their particles. Consequently, all the trial results have a different slump ratio. The deformation of each slump was 8.5 mm, 8.8mm, and 12mm for trials 5, 8 and 12, respectively. It is noteworthy that trial 8 has a lower slump than trial 5, with the difference likely due to the amount of *w/c* and superplasticizer in this mortar mix. It is also interesting that the mixing time and the time taken to pour into the slump have a great influence on the resulting mix. Each trial was, therefore, mixed for 5 minutes. As a result, trial 5 was expected to achieve higher penetration than trial 8, but trial 5 was more coherent than trial 8, as explained in the squeeze flow test, see Figure (15) and (16).

Figure (15) Mini-cone slump test for trial 8.

Figure (16) Spread-flow test: (a) for trial 5 which did not use fibre; (b) for the same trial by adding fibre with 1% polypropylene fibre.

Table 5 shows the results of the relative slump for all main mixes which were used for the printed samples. The minimum flow and slump occur in trial number 5 with 1% polypropylene fibre, which was expected due to the consistency and cohesiveness of this mix and the fibre content. The use of polypropylene fibre increased the mechanical strength of the structural element (section 4.1) and it reduced flowability (Figure 16) and shrinkage (Figure 14). In addition, fibre increases the buildability of the mortar and stiffens the mass of the printed layer. For that reason, it is

recommended that fibres be used in the printed specimens to increase stiffness and mitigate shrinkage in the printed part.

Table (5) The relative slump value and height of the slump for selected trials.

Trial no.	Height of slump (mm)	Diameter no. 1 (mm)	Diameter no. 2 (mm)	Relative slump value
Trial 5	8.5	190.63	184.65	2.52
Trial 5 (with 1% PP fibre)	6	148.27	155.25	1.30
Trial 8	8.8	199.52	201.84	3.02
Trail 12	12	201	201	3.04

4.1.2 Squeeze flow test

The results of the squeeze flow tests showed different values in the single, double and triple layers for each of the selected trial mixtures (5, 8, 12), as shown in Figure (17). In the single layer mortar mix test, higher results were obtained in the reaction force value until it reached the required displacement. For instance, at a displacement of 2.99mm, the required loads in trial 12 (concrete mix with small aggregate) were approximately 956.51 N. While at the same displacement for trials 5 and 8 (cement mortar), the load was approximately 277.82 N and 153.11 N, respectively. An examination of the results of the tests that utilised a double layer found significant differences in comparison to the single layer results. Trial 5 (cement mortar) had a reaction force which reached approximately 622.54 N when the displacement was about 3.99 mm, while for trials 12 and 8 the loads were 536.05 N and 275.75 N, respectively. At the same displacement, the results for the triple layers exhibited a similar pattern.

These results show that the mortar is more coherent than the concrete mixtures in the fresh state. Thus, it does not allow trapped air bubbles to remain in the mortar mixture. This is consistent with the study by Surendra, et al. [42], who discovered that the mortar in the first 24 hours had a greater compressive strength by comparison with normal concrete. Hence, a much higher percentage of open pores will exist in the concrete mixtures by comparison with the cementitious mortar due to the presence of aggregates. The larger particle sizes lead to a higher porosity within the concrete mixtures.

The reaction force is dependent on the number of chains (layers) and the force between the particles. Trial 12, a single layer test, showed that the presence of the small aggregate in the mixture can resist more force over the given displacement, Figure (17). Furthermore, Figure (17) shows that the mortar mix for more than one layer has better resistance than the concrete mix and that less penetration will occur between layers when the loads are applied (Figure 17).

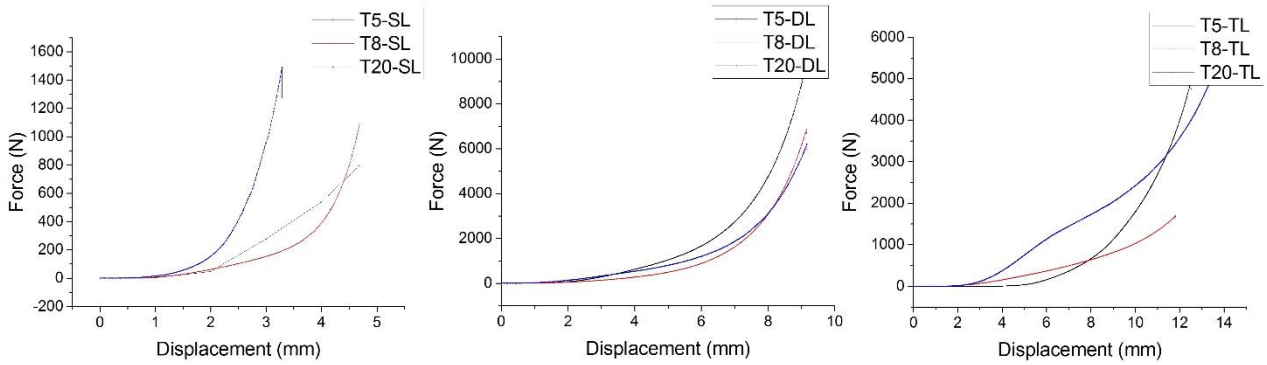

Figure (17) Single layer (SL), double layer (DL), and triple layers (TL) for the trials (5,8,12).

4.1.3 Setting time

In Table (6), the setting time results for the different trial mixes is shown. There are minimal differences in the initial setting times of these trials.

Table (6) The setting time results for the three main trials.

Trial No	Initial setting time (min)	Final setting time (min)
T5	75	120
T8	85	225
T12	75	90

The setting time has a crucial effect on the bond between printed layers and penetration rate between each printed layer.

The buildability tests, which depend on the setting time, have been applied for each trial by printing using an extrusion caulking gun.

Table (7) relates to trial 5, this trial was based on the original mix design, which used a 1:1 cement to fine sand ratio with a water/cement ratio of 0.33. This is able to be printed with the caulking gun and a circular nozzle of 14mm diameter. The settling observed was, to some extent, expected with the relatively similar levels of sand and cement in the mix. Not much change was observed in the heights of the sample. Sample number 6 showed a failed extrusion as it had collapsed considerably.

Table (7) Caulking gun extrusion nozzle (Ø14mm).

Time	**Buildability**						**Height (mm)**					
	1	2	3	4	5	6	1	2	3	4	5	6
15	×	×	×	×	×	×	12	11.5	12	12	12.5	8*
30	×	×	×	×	×	-	-	-	-	-	-	-
45	✓	✓	✓	✓	✓	-	-	-	-	-	-	-
*Failed extrusion.												

4.1.4 Compressive strength test

For each of the optimum trials that were printed successfully, a uniaxial compressive strength test was conducted. Figure (18) presents the results of the test conducted for the manual concrete mix,

which included polypropylene fibres with a different ratio.

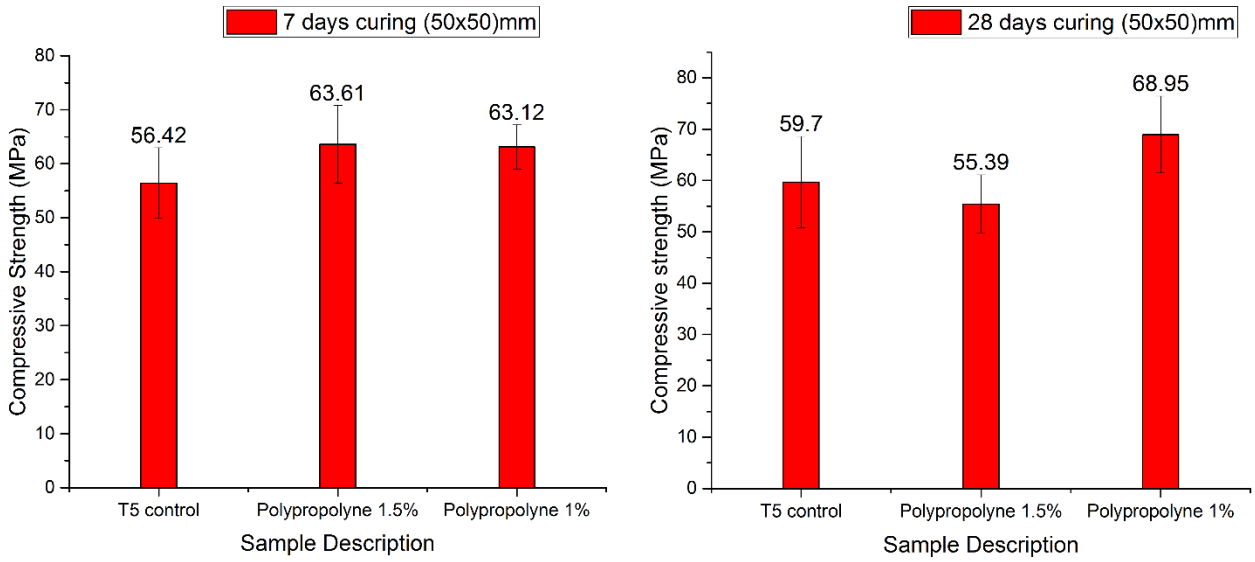

Figure (18) Compressive for manual concrete mix after 7-day and 28-day curing (the values Specify the actual strengths).

The printed short column was tested using the uniaxial loading test. The mix design and detail of the materials' properties are described in Table (14).

The compression strength result for the 7 layers of the printed mortar is shown in Figure (19). It can be observed that the highest compression result for printed mortar without curing and after 28 days was 13.45 kN as a maximum load. The printed specimens were left in the control temperature room at 20±2°C without any extra post-curing.

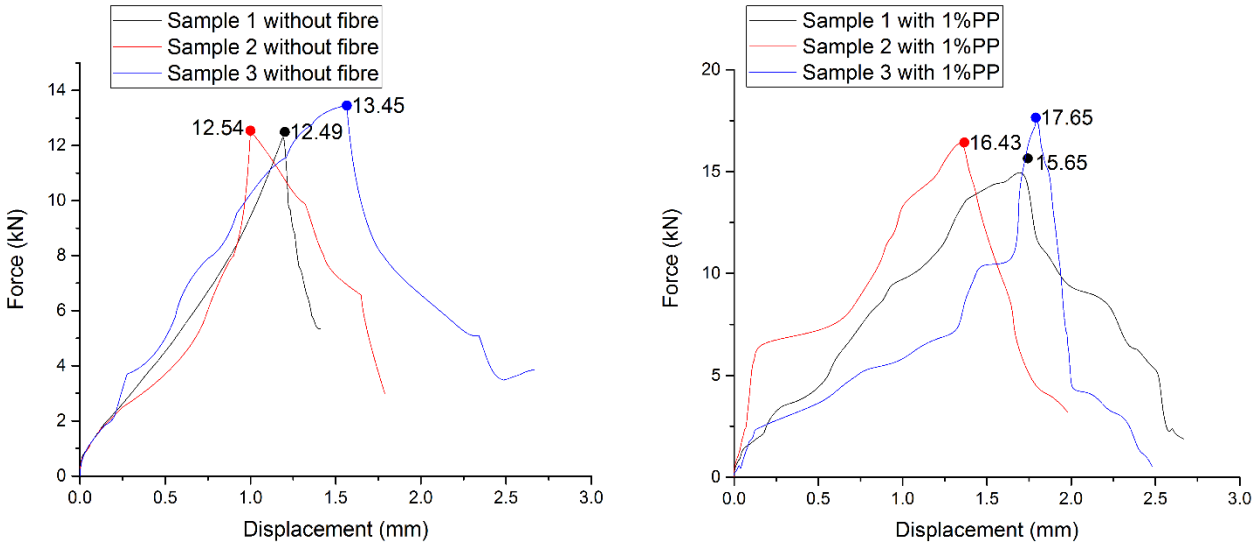

Figure (19) Results after 28 days for the short column (7 layers) without any time lapse between printed layers and without post-curing.

Figure (20) shows the printed sample after drying at the control temperature in the lab. No shrinkage cracks or hairline cracks on the printed specimens resulted. After loading, cracks appeared on the

edge of the printed column, as shown in Figure (20b). The results for the printed column showed that the average rate of the printed column is (12.83±0.54 kN). This is equal to the strength of 2.37 MPa, however, this needs to be improved by post-curing and the use of large particle sizes. It is also obvious that the low strength was due to the number of layers. The printed column was a mortar mix rather than a concrete mix which normally has less resistance than normal concrete after curing for 28 days.

Figure (20) (a) Printed specimen after drying at lab temperature; (b) Printed specimen under uniaxial load.

The short column under the uniaxial load cracked and ruptured at the edge of the sample, which showed the weakest part of the column. The edge of the column was revealed as the weakest part of the column due to the irregular movement of the robot while printing the column.

4.1.5 Flexural strength test

The three-point bending test was applied for the optimum mix of mortar using a different type of fibre and different ratios. The flexural strength results for the different ratios are shown in Figure (21).

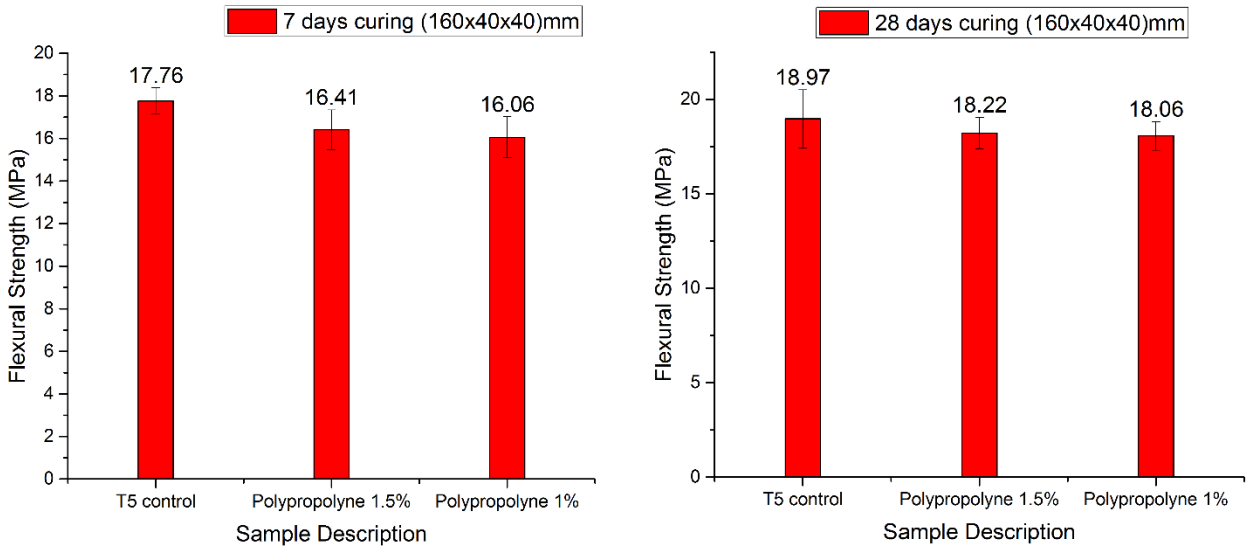

Figure (21) Flexural strength of manual concrete mix after 7-day and 28-day curing (the values specify the actual strengths).

The three-point bending test and flexural strength for the one, two, three and four layers of cementitious mortar with 1%PP fibre and without fibre are shown in Figure (22). The maximum result of 5.78 MPa for 28 days curing was observed in the single layer with 1% PP fibre content in the sample. Another high result was achieved for three printed layers which recorded 5.65 MPa. It is worth noticing that using PP fibre increased the flexural strength in all variable layers. In addition, it is noticeable that when increasing the number of layers, the flexural strength decreases due to inconsistency, a high ratio of moisture content and air trapped between layers.

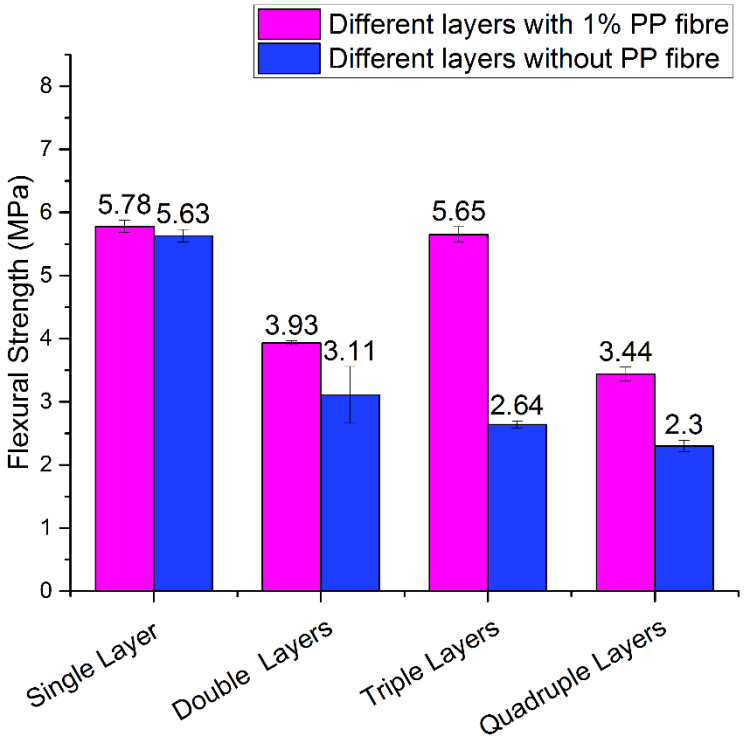

Figure (22) Flexural strength for the (1,2,3,4) layers of mortar mix with 1% PP fibre and without fibre for a circular nozzle of 14mm after 28 days stored in controlled laboratories at the desired temperature.

Figure (23) shows the effect of different nozzles on the result of flexural strength. It is noted that the highest flexural strength is in the 3rd printed layer of the rectangular nozzles when investigating the highest flexural strength in circular and rectangular nozzles in the wet medium cure. In Figure (23) all the layers of the rectangular nozzle have a similar result, but for the circular nozzle each layer has unstable results. Therefore, it shows that the load distribution of the circular nozzle is reduced with the reduced surface area and width. This directly affected the mechanical strength results of the printed object, see Figure (9). Consequently, the result suggests that a rectangular or square shape has a constant result and a better result than a circular nozzle print. This is consistent with the study of [20]. Conversely, it has been shown that wet medium curing is better than curing at air-temperature in vitro, as demonstrated by [43], Figure (23). In addition, it is highly recommended to use fly ash in the mix to reduce the voids between particles and increase the durability of the mortar [44].

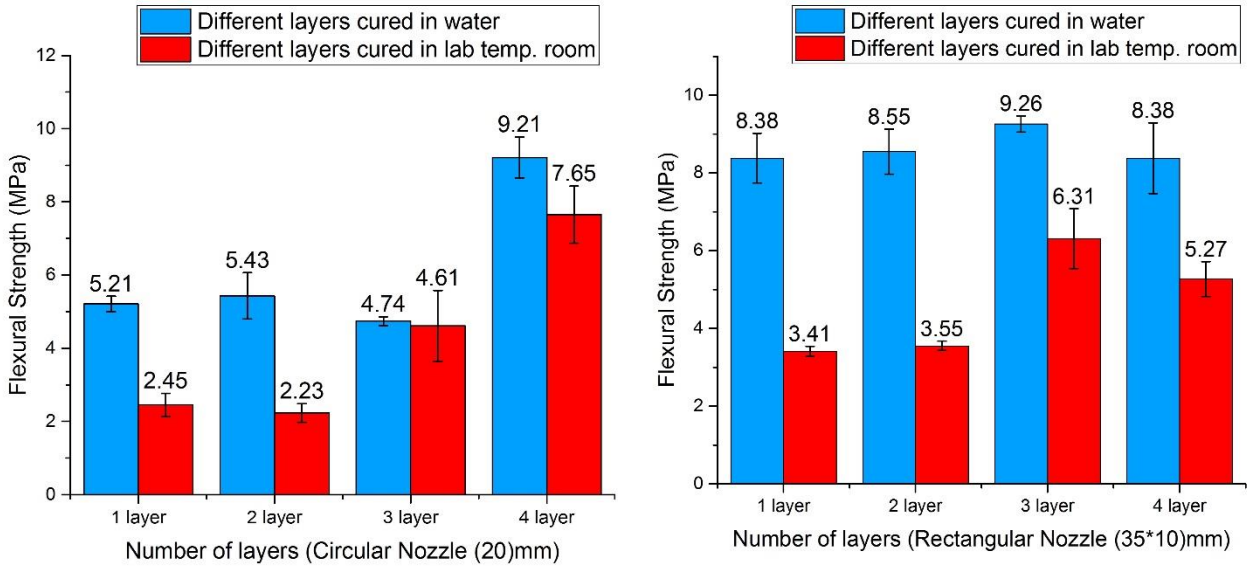

Figure (23) Flexural strength for the (1,2,3,4) layers of mortar mix for a circular nozzle (20)mm and a rectangular nozzle (35×10)mm at air temperature and with water curing.

5 CONCLUSIONS

This paper presents an investigation of extrusion printing involved in developing 3D printed mortar and concrete geometries using a 6DOF Industrial Robot. Different mix designs, which are used to optimize cementitious mix design with different delivery systems, were discussed. In addition, how these mixes have been evaluated by numerous trials and tests were explained in detail. Furthermore, it was found that optimisation of the cementitious mixes has a significant impact on the structure created" by the robot. The results show that mortar is more suitable and efficient for printing and construction of layers due to the smaller number of voids and less porosity between particles, while the concrete mixes with large particles allow more openings and internal porosity due to trapped air. Thus, printed specimens need to be cured using advanced technologies for different media to contribute to AM technology to print mortar members. The main contributions of the paper are:

- Validation of the optimum mix proportions in conjunctions with the different delivery mechanism for printing cementitious slurry.
- Presents limitations and challenges inherent to this printing process.
- Comparison of different sized and rectangle- and circle-shaped printer nozzles, for a variety of layer thickness and heights.
- Relative slump, spread-flow and squeeze flow tests for the optimum mix

It is recommended that for upcoming studies, the focus should be on predictive models, feedback to reduce the chance of errors and online sensing to integrate more online coincidences for the robot. It is also recommended that different waiting time intervals between layers be investigated, as well as checks of the different heights of the nozzles from the platform.

ACKNOWLEDGEMENT

The authors would like to express their sincere gratitude to Sika Australia for supplying chemical materials and Elasto Plastic Concrete for providing the polypropylene fibre. The authors would like to thank TAFE Ultimo for allowing their facilities to be used.

6 REFERENCES

1. Buswell, R. A.; Soar, R.; Gibb, A. G.; Thorpe, T., The potential of freeform construction processes. **2005**.
2. Edwards, L.; Holt, C.; Keyte, L.; Lloyd, R., Construction 3D Printing. In *Concrete 2013*, Gold Coast, Australia 2015.
3. Junk, S.; Sämann-Sun, J.; Niederhofer, M. In *Application of 3D Printing for the Rapid Tooling of Thermoforming Moulds*, Proceedings of the 36th International MATADOR Conference, 2010; Springer: pp 369-372.
4. Kwon, H. Experimentation and analysis of contour crafting (CC) process using uncured ceramic materials. University Of Southern California, 2002.
5. Lipson, H.; Kurman, M., *Fabricated: The new world of 3D printing*. John Wiley & Sons: New York, USA 2013.
6. Sachs, E.; Cima, M.; Williams, P.; Brancazio, D.; Cornie, J., Three dimensional printing: rapid tooling and prototypes directly from a CAD model. *Journal of Engineering for Industry* **1992,** 114, (4), 481-488.
7. Buswell, R. A.; Leal de Silva, W. R.; Jones, S. Z.; Dirrenberger, J., 3D printing using concrete extrusion: A roadmap for research. *Cement and Concrete Research* **2018,** 112, 37-49.
8. Lowke, D.; Dini, E.; Perrot, A.; Weger, D.; Gehlen, C.; Dillenburger, B., Particle-bed 3D printing in concrete construction – Possibilities and challenges. *Cement and Concrete Research* **2018**.
9. Le, T. T.; Austin, S. A.; Lim, S.; Buswell, R. A.; Gibb, A. G. F.; Thorpe, T., Mix design and fresh properties for high-performance printing concrete. *Materials and Structures* **2012,** 45, (8), 1221-1232.
10. Pegna, J., Exploratory investigation of solid freeform construction. *Automation in Construction* **1997,** 5, (5), 427-437.
11. Khoshnevis, B.; Bukkapatnam, S.; Kwon, H.; Saito, J., Experimental investigation of contour crafting using ceramics materials. *Rapid Prototyping Journal* **2001,** 7, (1), 32-42.
12. Christ, S.; Schnabel, M.; Vorndran, E.; Groll, J.; Gbureck, U., Fiber reinforcement during 3D printing. *Materials Letters* **2015,** 139, 165-168.
13. Compton, B. G.; Lewis, J. A., 3D ‐ printing of lightweight cellular composites. *Advanced materials* **2014,** 26, (34), 5930-5935.
14. Hambach, M.; Volkmer, D., Properties of 3D-printed fiber-reinforced Portland cement paste. *Cement and Concrete Composites* **2017,** 79, 62-70.
15. Ogura, H.; Nerella, V.; Mechtcherine, V., Developing and testing of strain-hardening cement-based composites (SHCC) in the context of 3D-printing. *Materials* **2018,** 11, (8), 1375.

16. Bos, F.; Wolfs, R.; Ahmed, Z.; Salet, T., Additive manufacturing of concrete in construction: potentials and challenges of 3D concrete printing. *Virtual and Physical Prototyping* **2016,** 11, (3), 209-225.
17. Paul, S. C.; van Zijl, G. P.; Tan, M. J.; Gibson, I., A review of 3D concrete printing systems and materials properties: Current status and future research prospects. *Rapid Prototyping Journal* **2018**, (just-accepted), 00-00.
18. Lim, S.; Buswell, R. A.; Le, T. T.; Wackrow, R.; Austin, S. A.; Gibb, A. G. F.; Thorpe, T., Development of a viable concrete printing process. **2011**.
19. Le, T. T.; Austin, S. A.; Lim, S.; Buswell, R. A.; Law, R.; Gibb, A. G.; Thorpe, T., Hardened properties of high-performance printing concrete. *Cement and Concrete Research* **2012,** 42, (3), 558-566.
20. Perrot, A.; Rangeard, D.; Courteille, E., 3D printing of earth-based materials: Processing aspects. *Construction and Building Materials* **2018,** 172, 670-676.
21. Gosselin, C.; Duballet, R.; Roux, P.; Gaudillière, N.; Dirrenberger, J.; Morel, P., Large-scale 3D printing of ultra-high performance concrete – a new processing route for architects and builders. *Materials & Design* **2016,** 100, 102-109.
22. Hamad, A. J., Size and shape effect of specimen on the compressive strength of HPLWFC reinforced with glass fibres. *Journal of King Saud University - Engineering Sciences* **2017,** 29, (4), 373-380.
23. Paul, S. C.; van Zijl, G. P. A. G.; Tan, M. J.; Gibson, I., A review of 3D concrete printing systems and materials properties: current status and future research prospects. *Rapid Prototyping Journal* **2018,** 24, (4), 784-798.
24. Anell, L. Concrete 3d printer. Master Thesis, Lund University, Sweden, 2015.
25. Al-Qutaifi, S.; Nazari, A.; Bagheri, A., Mechanical properties of layered geopolymer structures applicable in concrete 3D-printing. *Construction and Building Materials* **2018,** 176, 690-699.
26. Soltan, D. G.; Li, V. C., A self-reinforced cementitious composite for building-scale 3D printing. *Cement and Concrete Composites* **2018,** 90, 1-13.
27. Shakor, P.; Renneberg, J.; Nejadi, S.; Paul, G., Optimisation of Different Concrete Mix Designs for 3D Printing by Utilising 6DOF Industrial Robot. In *ISARC. Proceedings of the International Symposium on Automation and Robotics in Construction*, Vilnius Gediminas Technical University, Department of Construction Economics & Property: Taipei, Taiwan, 2017; Vol. 34.
28. ASTMC1437, Standard Test Method for Flow of Hydraulic Cement Mortar. 2015.
29. ABNT-NBR15839, Argamassa de assentamento e revestimento de paredes e tetos – caracterização reológica pelo método Squeeze-flow. 2010.
30. ASTMC191-13, Standard Test Methods for Time of Setting of Hydraulic Cement by Vicat Needle. ASTM: 2013.
31. Sleiman, H.; Perrot, A.; Amziane, S., A new look at the measurement of cementitious paste setting by Vicat test. *Cement and Concrete Research* **2010,** 40, (5), 681-686.
32. AS1012.9:2014, Methods of testing concrete - Compressive strength tests - Concrete, mortar and grout specimens. 2014.
33. ASTMC293/C293M, 293 Standard Test Method for Flexural Strength of Concrete (Using Simple Beam With Center-Point Loading). *ASTM Standard* **2002**.
34. de Vicente, J.; Ruiz-López, J. A.; Andablo-Reyes, E.; Segovia-Gutiérrez, J. P.; Hidalgo-Alvarez, R., Squeeze flow magnetorheology. *Journal of Rheology* **2011,** 55, (4), 753-779.
35. Cyr, M.; Legrand, C.; Mouret, M., Study of the shear thickening effect of superplasticizers on the rheological behaviour of cement pastes containing or not mineral additives. *Cement and Concrete Research* **2000,** 30, (9), 1477-1483.
36. Li, X.; Zhou, R.; Yao, W.; Fan, X., Flow characteristic of highly underexpanded jets from various nozzle geometries. *Applied Thermal Engineering* **2017,** 125, (Supplement C), 240-253.
37. Cwalina, C. D.; Harrison, K. J.; Wagner, N. J., Rheology of cubic particles suspended in a Newtonian fluid. *Soft Matter* **2016,** 12, (20), 4654-4665.

38. Böhmer, M. R.; Schroeders, R.; Steenbakkers, J. A. M.; de Winter, S. H. P. M.; Duineveld, P. A.; Lub, J.; Nijssen, W. P. M.; Pikkemaat, J. A.; Stapert, H. R., Preparation of monodisperse polymer particles and capsules by ink-jet printing. *Colloids and Surfaces A: Physicochemical and Engineering Aspects* **2006,** 289, (1), 96-104.
39. Crowley, S. V.; Gazi, I.; Kelly, A. L.; Huppertz, T.; O'Mahony, J. A., Influence of protein concentration on the physical characteristics and flow properties of milk protein concentrate powders. *Journal of Food Engineering* **2014,** 135, (Supplement C), 31-38.
40. Feys, D.; Verhoeven, R.; De Schutter, G., Why is fresh self-compacting concrete shear thickening? *Cement and Concrete Research* **2009,** 39, (6), 510-523.
41. Fitzpatrick, J. J.; Barringer, S. A.; Iqbal, T., Flow property measurement of food powders and sensitivity of Jenike's hopper design methodology to the measured values. *Journal of Food Engineering* **2004,** 61, (3), 399-405.
42. Surendra, P. S.; Yilmaz, A.; Thomas, V., Determination of Early Age Mortar and Concrete Strength by Ultrasonic Wave Reflections. **2003**.
43. Mindess, S.; Young, J. F.; Darwin, D., Concrete, prentice hall. *Englewood Cliffs, NJ* **1981,** 481.
44. Kurda, R.; de Brito, J.; Silvestre, J. D., Combined influence of recycled concrete aggregates and high contents of fly ash on concrete properties. *Construction and Building Materials* **2017,** 157, 554-572.